



Repositorio Institucional de la Universidad Autónoma de Madrid

<https://repositorio.uam.es>

Esta es la **versión de autor** del artículo publicado en:

This is an **author produced version** of a paper published in:

Nuclear Instruments and Methods in Physics Research, Section B: Beam Interactions
with Materials and Atoms 371 (2016): 116 - 120

DOI: <http://dx.doi.org/10.1016/j.nimb.2015.08.080>

Copyright: © 2015 Elsevier B.V.

El acceso a la versión del editor puede requerir la suscripción del recurso

Access to the published version may require subscription

Analytical simulation of RBS spectra of nanowire samples

Nuno P. Barradas ¹, C. García Núñez ², A. Redondo-Cubero ^{2,3}, G. Shen ⁴, P. Kung ⁴, J.L. Pau ²

¹ Centro de Ciências e Tecnologias Nucleares, Instituto Superior Técnico, Universidade de Lisboa, E.N. 10 ao km 139,7, 2695-066 Bobadela LRS, Portugal

² Laboratorio de Electrónica y Semiconductores, Departamento de Física Aplicada, Universidad Autónoma de Madrid, 28049 Madrid, Spain

³ Centro de Micro-Análisis de Materiales, Universidad Autónoma de Madrid, 28049 Madrid, Spain

⁴ Department of Electrical and Computer Engineering, The University of Alabama, AL 35487, USA

Abstract. Almost all, if not all, general purpose codes for analysis of Ion Beam Analysis data have been originally developed to handle laterally homogeneous samples only. This is the case of RUMP, NDF, SIMNRA, and even of the Monte Carlo code Corteo. General-purpose codes usually include only limited support for lateral inhomogeneity. In this work, we show analytical simulations of samples that consist of a layer of parallel oriented nanowires on a substrate, using a model implemented in NDF. We apply the code to real samples, made of vertical ZnO nanowires on a sapphire substrate. Two configurations of the nanowires were studied: 40 nm diameter, 4.1 μm height, 3.5% surface coverage; and 55 nm diameter, 1.1 μm height, 42% surface coverage. We discuss the accuracy and limits of applicability of the analysis.

1. Introduction

Ion Beam Analysis (IBA) techniques such as Rutherford backscattering spectrometry (RBS) have excelled at providing reliable quantitative information on the composition and elemental depth profile of samples of all provenances. RBS almost always uses a broad beam, with

dimension commonly around 1 mm^2 , or in that order of magnitude. In the presence of 2D and 3D structures, including inclusions, lateral heterogeneity, and surface and interface roughness, broad beam RBS measures an average of all the structures present in the area of the beam spot. This has been successfully utilised to make quantitative studies of roughness [1-3], inclusions [4,5], and even quantum dots [6] with RBS.

Specific codes such as MAST [7-11], PowerMeis [12,13], and others [14] exist that can handle 3D samples, including simulation of the spectra expected from user-input structures. These codes usually calculate spectra for all possible trajectories of the analysing ions in the 3D sample, and produce an average that can be directly compared to the experimental data. This is accurate and slow. General-purpose codes such as NDF [15], SIMNRA [16], and even the Monte Carlo code Corteo [17], are however geared to handle laterally homogeneous samples. They include only limited support for lateral inhomogeneity. This can be via a user-input distribution of the thickness of given layers, or via approximate models of surface and interface roughness. NDF and SIMNRA provide some support for the influence of inclusions and quantum dots on energy spectra. Corteo and SIMNRA versions presented in this conference can handle laterally inhomogeneous samples. In this work, we show fast analytical simulations of samples that consist of a layer of parallel oriented nanowires on a substrate, using a model implemented in NDF. We apply the code to real samples, made of vertical ZnO nanowires on a sapphire substrate. Two configurations of the nanowires were studied: 40 nm diameter, 4 μm height, 3.5% surface coverage; and 55 nm diameter, 1 μm height, 42% surface coverage. We discuss the accuracy and limits of applicability of the analysis.

2. Experimental details

ZnO nanowires are grown by chemical vapour deposition in a horizontal quartz tube furnace via a carbothermal reduction of ZnO powder and in an oxidizing ambient. Zn source consists of a ZnO/C powder mixture with a 1/2 mass ratio and a total mass of 1.5 g. The substrate is a *c*-plane sapphire covered with a ZnO 7 nm thick seed layer; the specific deposition procedure of this ZnO layer is thoroughly described elsewhere [18]. Nanowires were grown at pressures of 1 atm (sample A), and 0.67 atm (sample B), measured by a pressure gauge placed at an equivalent sample position during a calibration stage. Both processes are carried out under a constant Ar/O₂ gas flux of 47 sccm, consisting of only 2 vol.% of O₂ diluted in Ar. The seed layer areal density is only about 6% and 1.5% of the total ZnO areal density in samples A and B, respectively.

The use of different growth pressures allows to control resultant nanowire morphology; morphological characteristics of nanowires are analyzed by means of scanning electron microscopy (SEM) with a 15 keV energy (Figure 1), including nanowire average diameter and length, nanowire surface coverage (defined as the fraction of the surface area covered by nanowires). SEM images taken at 0° with respect to the sample surface (Figure 1(a,c)), i.e. the electron beam is aligned to the nanowire edge, are used to estimate the average nanowire diameter and the surface coverage. The former is calculated taking into account the diameter of around 50 nanowires, resulting in an average diameter of 40 and 55 nm for samples A and B, respectively. From Figure 1(a,c), one can also extract the surface coverage, taking into account the number of nanowires per area, and the cross-sectional area of a single nanowire. In sample A, SEM image shows a nanowire surface density of around 7 nanowires per μm^2 (Figure 1(a)); assuming an average nanowire cross-section of $5 \times 10^{-3} \mu\text{m}^2$, corresponding to a nanowire with a diameter of 40

nm, the surface coverage is about 3.5%. Following the same analysis for sample B, the obtained surface coverage is about 42%. Figure 1(b) and (d) are SEM images taken at 90° with respect to the nanowire growth direction, allowing to estimate the average nanowire length; for samples A and B the average nanowire length results in values around 4.13 and 1.15 μm , respectively.

RBS measurements were performed at the Center of Micro-Analysis of Materials. The sample was mounted on a high-precision (0.01°) three axis goniometer inside a vacuum chamber (10^{-6} mbar), so the orientation of the sample surface relative to the incident beam can be precisely controlled. Backscattered ions were detected with a Si-barrier detector located at 170° scattering angle (energy resolution of 15 keV). In order to enhance the sensitivity to O, RBS was carried out under $^{16}\text{O}(\alpha,\alpha)^{16}\text{O}$ resonant conditions [19], with a 3055 keV $^4\text{He}^{2+}$ beam. Different RBS measurements were carried out with the detector located at a 170° scattering angle in the IBM geometry, involving angles between the incident ion beam and the normal to the sample surface, ranging from 0° to 70°, which correspond, to 10° to 80° exit angles relative to the normal to the surface. To avoid channeling in the substrate each spectrum is the sum of 200 low-dose spectra recorded during the combined movement of theta and tilt angles within a short range of 2°. Both theta and tilt are moved describing a circumference around the normal direction of the sample at 0°. This procedure warrants a reproducible random spectrum averaging over many directions that are close to 0° [20].

3. Model and calculations

We developed and presented previously an approximate way to include the effect of lateral inhomogeneity in analytical simulations of IBA data [21,22]. The main idea is to realise that roughness leads to a broadening of signals such as peaks or interfaces, in a similar way that

energy straggling does. The broadening due to roughness can be calculated, and included as an extra contribution to the energy spread Ω of the detected beam:

$$\Omega^2 = \Omega_{\text{system}}^2 + \Omega_{\text{straggling}}^2 + \Omega_{\text{sample}}^2, \quad (1)$$

where Ω_{system} is the system resolution, $\Omega_{\text{straggling}}$ is the straggling (including energy loss straggling, multiple scattering, and geometrical straggling) that we calculate with the code DEPTH [23,24], and Ω_{sample} is the energy spread induced by sample features. We previously developed models to calculate Ω_{sample} for different types of roughness [3,21] and inclusions [6], and included it in NDF. One of the advantages of this approach is that the computation times are not significantly increased, because the calculation of Ω_{sample} is very quick.

One of the models was for columnar inclusions [6], following the work by Stoquert and Szörenyi [4], which assumed a Gaussian distribution for spherical inclusions. Mayer et al. showed [5] that for high density of spherical inclusions, non-Gaussian distributions are more appropriate. A similar argument can be made for columnar inclusions, and therefore the model implemented in NDF is valid for low densities. For higher densities of the columnar inclusions, the calculations are expected to become less accurate. Nevertheless, no alternative or more accurate model has been presented so far.

Voids are a special case for simulation. In principle, there is no measurable signal coming from voids, since there is no scattering and no energy loss in voids. However, they are included in several ways in the simulation, as discussed in detail by Stoquert and Szörenyi [4]. First, each beam particle crosses a different number of voids as they traverse a layer where voids and matter coexist. This leads to a spread in the energy loss, which in turn leads to the energy spread Ω_{sample} in Eq. (1). Then, simulations require the total quantity of matter present. When using other

techniques such as microscopy to determine the size of structures, and from that determine the quantity of matter, the void fraction, and therefore the matter fraction, is an important quantity.

This is illustrated in Figure 2, where we show simulations for supposed Au nanowires with 20 nm diameter and 1, 2, and 4 μm height, on a light substrate (C was used in the simulations, only the Au signal is shown in the figure). The Au nanowires occupy in all cases a 10% volume fraction. The simulations are made for a 2 MeV ^4He beam at 25° incidence, detected at an 170° scattering angle. For the same volume fraction, an increased height of the nanowires corresponds to a larger quantity of matter, that is, a larger Au areal density. At the same time, the energy spread also increases, because the thickness of the "layer" with nanowires is larger and hence leads to a progressively larger dispersion of paths of the ion particles.

One should note that the model to calculate Ω_{sample} is based on a statistical analysis of the paths of the beam ions on the voids and on the nanowires. The analysis includes the spread in number of nanowires crossed by each particle, and the different possible paths within a nanowire. When the beam is nearly aligned with the structures, this fails. For instance, for perfectly columnar nanowires perpendicular to the surface, at normal incidence, each incoming beam particle has a path either entirely inside a nanowire, or entirely in the void. This is a binary distribution that is very far removed from the Gaussian distribution assumed in the model. Therefore, at angles near normal incidence, the model will fail. We do not have a general model to predict the minimum angle of incidence for which the model is valid. We compared NDF calculations with data previously analysed by the fully 3D MAST code [25]. The sample was thick porous alumina, with perpendicular pores with diameter around 45 nm, measured with a 3.2 MeV ^4He beam. NDF simulations reproduced the data well for tilt angles near or above 10°

and up to 60°. In the general case, however, one should always collect data at different angles of incidence, ensuring consistency in the data analysis.

Finally, the model is developed for perfectly cylindrical and perfectly aligned structures, all of the same diameter and width. In real samples, there is often a distribution of shapes and sizes that will lead to an extra energy spread of the beam.

4. Results and discussion

The RBS spectra of sample A (40 nm diameter, 4 µm height and 3% volume fraction) are shown in Figure 3. Simulations made using Eq. (1) are shown as solid lines. They were done for nearly the nominal conditions: 40 nm diameter, 3.92 µm height and 2.8% volume fraction. To achieve the optimal simulations, the 40 nm diameter was assumed fixed, and the volume fraction was adjusted. The height is derived from the volume fraction together with the total quantity of matter, that can be determined from the experiments. Some roughness was also included in the simulation, to account for the spread in nanowire height and orientation observed in Figure 3. To convert from thickness to areal density, the bulk density of ZnO was used. The simulation at normal incidence does not reproduce the data, not even its general features. This was expected, because at normal incidence the incoming beam particles can have a path always inside a nanowire, leading to very large energy losses. Indeed, the low energy tail of the Zn signal extends to lower energies than at 20° or even 45° incidence. At 20°, there is still a misfit. The spectra at 45°, 60° and 70° are well simulated. This underpins the importance of collecting data for a wide range of angles.

The RBS spectra of sample B (55 nm diameter, 1.1 µm height and 42% volume fraction) are shown in Figure 4. The simulations were done for 55 nm diameter, 1.12 µm height and 42%

volume fraction. In this case, extended roughness had to be introduced, with standard deviation of the nanowire height around 200 nm. This is expected, as it is observed in Figure 1 that for this sample there is a large variation in nanowire height. However, given the limitations of the nanowire model for large volume fraction values, the extra roughness introduced may be an artefact of the simulation. As in sample A, the normal incidence spectrum is poorly fitted, because the model breaks down for small tilt angles. The other spectra, from 20° to 70°, are well fitted with nanowire parameters close to the nominal values. Again, this demonstrates the need to collect spectra at different experimental geometries.

To emphasize this point, we made a simulation to the spectrum at normal incidence by assuming a continuous ZnO layer with roughness, modelled via a distribution of thickness. We adjusted the thickness distribution until a good fit to the 0° spectrum was obtained. The thickness distribution so derived is shown in Figure 5; **Error! No se encuentra el origen de la referencia..** It has a peak for low thickness values, around 90-150 nm, and extends to large values, slightly above 1 µm, which is much less than the nanowire height. The simulations made for the other angles using the same thickness distribution are also shown in Figure 3. They are clearly wrong, and confirm that the rough layer model is not valid. Instead, the nanowire model can be used, with the data at 45° and above, to analyse the data. We also made a fit to the 0° spectra using a distribution of thicknesses. The derived distribution, shown in Figure 5; **Error! No se encuentra el origen de la referencia..**, has a plateau at around 450-700 nm, and extends to 1400 nm, slightly more than the average nanowire height of 1100 nm.

In a sample with perfect nanowires, perfectly perpendicular to the surface, and with RBS done at 180° with an annular detector, the distribution would have one delta at 7 nm with ≈97% weight, corresponding to the ZnO seed layer thickness, and another delta at 4 µm with ≈3% for

sample A, corresponding to the nanowire height. This is because in that perfect case, 3% of the ions travel within a single nanowire until they reach the substrate. Thus, the expected spectrum for a perfect sample would have a wide low yield Zn plateau. Taking into account the ZnO seed layer, a small Zn surface peak yield would also be present. A slightly different spectrum is expected for a perfect sample but measured in normal incidence at a 170° angle of incidence, because the 3% of the incoming beam particles that travel entirely within a nanowire scatter at a 170° angle, and therefore are not in the same nanowire on the way out, although they may cross other nanowires on the way out leading to some further energy loss, but less than if the beam were always in the nanowire. In any case, the expected spectrum would be a wide low yield Zn plateau with a small surface peak. In the current experiment, the bending and variation of nanowire orientation, clearly observed in Figure 1, means that the ideal spectrum for perfect vertical nanowires cannot be observed. In fact, the strong peak in the thickness distribution shown in Figure 5; **Error! No se encuentra el origen de la referencia.** for sample A is approximately located at the average ZnO coverage (defined as the thickness of a uniform film with the same total amount of ZnO), which is 110 nm, which is consistent with a fairly disordered nanowire distribution. For sample B the nanowires are more similar to the perfect case, and the experimental normal incidence spectrum resembles more the shape for regular cylindrical structures calculated with Monte Carlo [12]. Also, the thickness distribution for sample B shown in Figure 5 does have a plateau, albeit near the average ZnO coverage, which is 470 nm. In any case, it is clear that the analytical simulations presented here cannot reproduce near normal-incidence data, even for fairly disordered nanowire distributions.

Finally, Pászti et al. [8] showed that, for a 3145 ^4He keV beam on oxidised porous Si samples, the shape and width of the resonance changed dramatically with the angle of incidence, and that

this could be well reproduced with MAST. In the experiments reported here, the change is much smaller. The reason is that in our case the initial beam energy is close to the 3037 keV resonance energy, and there is little extra energy spread due to the nanowires when the beam reaches the resonance energy.

5. Summary

We presented analytical simulations of RBS spectra of nanostructured samples, in particular of samples consisting of nanowires oriented perpendicularly to a substrate. The simulations are based on a model first developed by Stoquert and Szörenyi [4] for spherical inclusions, extended by us to cylindrical inclusions [6]. We discussed the limitations of the model. We then applied the model to ZnO nanowires on a sapphire substrate, measured with RBS at different angles of incidence. We discussed the results at the light of the model limitations. It was also made clear that one single spectrum is highly ambiguous, and that meaningful data analysis requires collecting a series of spectra, in this case at different angles of incidence. We conclude that, used with care, and provided that spectra are collected in a range of angles of incidence, the model can be used to validate a given supposed nanowire structure, and also to eliminate alternative sample structures. However, we stress that solving the reverse problem, of deriving the nanowire diameter, height and volume fraction from RBS data only, is not achievable in the general case, and would result in large uncertainties even in favourable cases.

Acknowledgements

In Memoriam of Feri Pászti, an extraordinary ion beam scientist who, amongst other more important works, developed the first analytical roughness models implemented in NDF, and

provided the first data to test the columnar inclusion algorithm implemented in NDF. Authors thank funding from projects CTQ2014-53334-C2-2-R (MINECO, Spain) and NANOAVANSENS S2013/MIT 3029 (Comunidad de Madrid). A.R.C. acknowledges Juan de la Cierva program (under contract number JCI-2012-14509). This work was partially funded by Fundação para a Ciência e Tecnologia under grant UID/Multi/04349/2013.

References

1. N.P. Barradas, A.P. Knights, C. Jeynes, O.A. Mironov, T. Grasby, and E.H.C. Parker, Phys. Rev. B 59 (1999) 5097.
2. M. Mayer, Nucl. Instrum. Methods Phys. Res. B 194 (2002) 177.
3. N. P. Barradas, E. Alves, S. Pereira, V. V. Shvartsman, A. L. Kholkin, E. Pereira, K. P. O'Donnell, C. Liu, C. J. Deatcher I. M. Watson, M. Mayer, Nucl. Instrum. Methods Phys. Res. B 217 (2004) 479.
4. J.P. Stoquert, T. Szörenyi, Phys. Rev. B 66 (2002) 144108.
5. M. Mayer, U. von Toussaint, J. Dewalque, O. Dubreuil, C. Henrist, R. Cloots, F. Mathis, Nucl. Instrum. Methods Phys. Res. B 273 (2012) 83.
6. N.P. Barradas, Nucl. Instrum. Methods Phys. Res. B 261 (2007) 435.
7. Z. Hajnal, E. Szilágyi, F. Pászti, and G. Battistig, Nucl. Instrum. Methods Phys. Res. B 118 (1996) 617.
8. F. Pászti, E. Szilágyi, Z. E. Horváth, A. Manuaba, G. Battistig, Z. Hajnal, and É. Vázsonyi, Nucl. Instrum. Methods Phys. Res. B 136-138 (1998) 533.
9. Z. Zolnai, A. Deák, N. Nagy, A. L. Tóth, E. Kótai, and G. Battistig, Nucl. Instrum. Methods Phys. Res. B 268 (2010) 79.
10. Z. Zolnai, N. Nagy, A. Deák, G. Battistig, E. Kótai, Phys. Rev. B 83 (2011) 233302.

11. Z. Zolnai, Appl. Surf. Sci. 281 (2013) 17.
12. M. A. Sortica, P. L. Grande, G. Machado, and L. Miotti, J. Appl. Phys. 106 (2009) 114320..
13. M. A. Sortica, P. L. Grande, C. Radtke, L. G. Almeida, R. Debastiani, J. F. Dias and A. Hentz, Appl. Phys. Lett. 101 (2012) 023110.
14. J. Gustafson A. R. Haire, and C. J. Baddeley, Surface Science 605 (2011) 220.
15. N.P. Barradas, C. Jeynes, M. Jenkin, and P.K. Marriott, Thin Solid Films 343-344 (1999) 31.
16. M. Mayer, AIP Conf. Proc. 475 (1999) 541.
17. F. Schiettekatte, Nucl. Instrum. Methods Phys. Res. B 266 (2008) 1880.
18. G. Shen, N. Dawahre, J. Waters, S.M. Kim, and P. Kung, J. Vac. Sci. Technol. B 31 (2013) 041803.
19. J.A. Leavitt, L.C. McIntyre, M.D. Ashbaugh, J.G. Oder, Z. Lin, and B. Dezfouly-Arjomandy, Nucl. Instr. and Meth. B 44 (1990) 260.
20. A. Redondo-Cubero, K. Lorenz, N. Franco, S. Fernández-Garrido, R. Gago, P. J. M. Smulders, E. Muñoz, E. Calleja and E. Alves, J. Phys. D: Appl. Phys. 42 (2009) 065420.
21. N.P. Barradas, J. Physics D: Applied Physics 34 (2001) 2109.
22. N.P. Barradas, Nucl. Instrum. Methods Phys. Res. B190 (2002) 247.
23. E. Szilágyi, F. Pászti, and G. Amsel, Nucl. Instrum. Methods B 100 (1995) 103.
24. E. Szilágyi, Nucl. Instrum. Methods B 161-163 (2000) 37.
25. Dr. Feri Pászti, private communication (2007). The results were never published.

Figure 1. SEM of ZnO nanowire samples A (40 nm diameter, 4 μm height and 3.5% volume fraction) and B (55 nm diameter, 1 μm height and 42% volume fraction). a) Top and b) lateral view of sample A, c) top and d) lateral view of sample B.

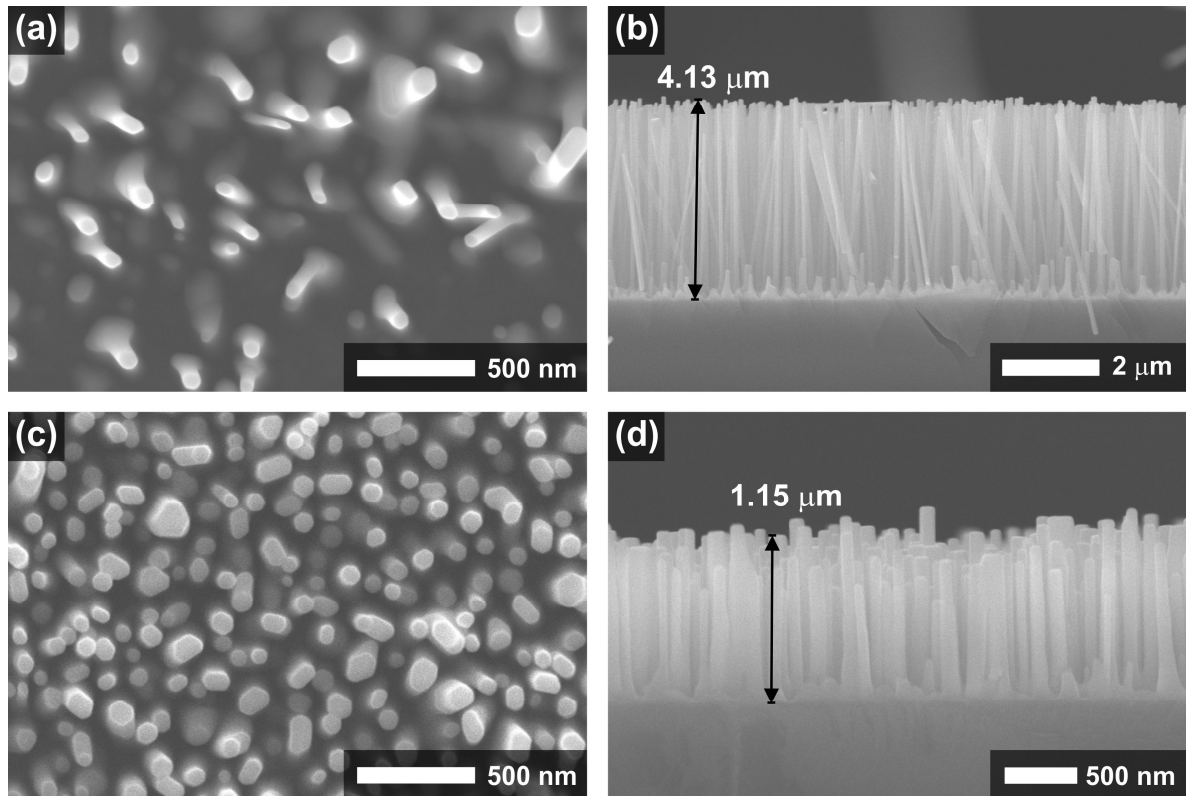


Figure 2. Simulations of RBS spectra of Au nanowires with 20 nm diameter and 1, 2, and 4 μm height, on a light substrate (C was used in the simulations, only the Au signal is shown). The Au nanowires occupy in all cases a 10% volume fraction. Simulations for homogeneous Au films with the same areal density are also shown as dashed lines.

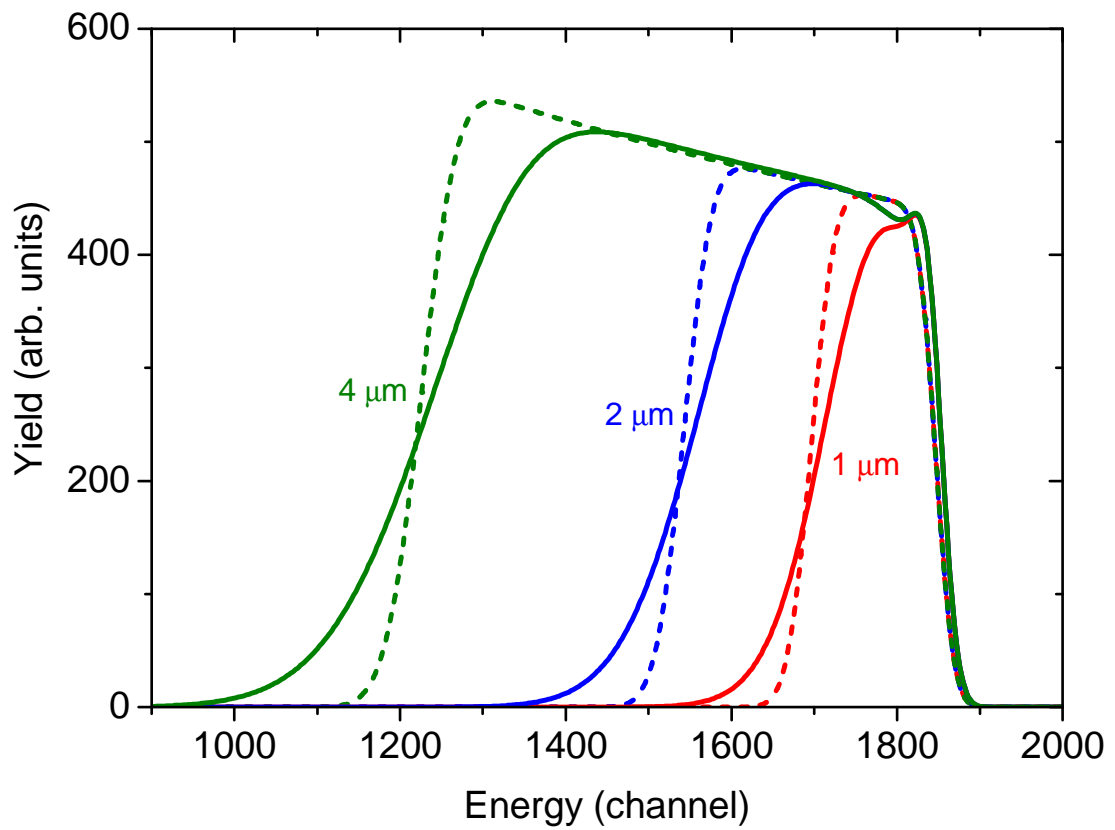


Figure 3. RBS spectra of ZnO nanowire sample A. Solid lines: simulation with nanowire model. Dashed lines: simulation using a rough but continuous ZnO layer with the thickness distribution given in **¡Error! No se encuentra el origen de la referencia..**

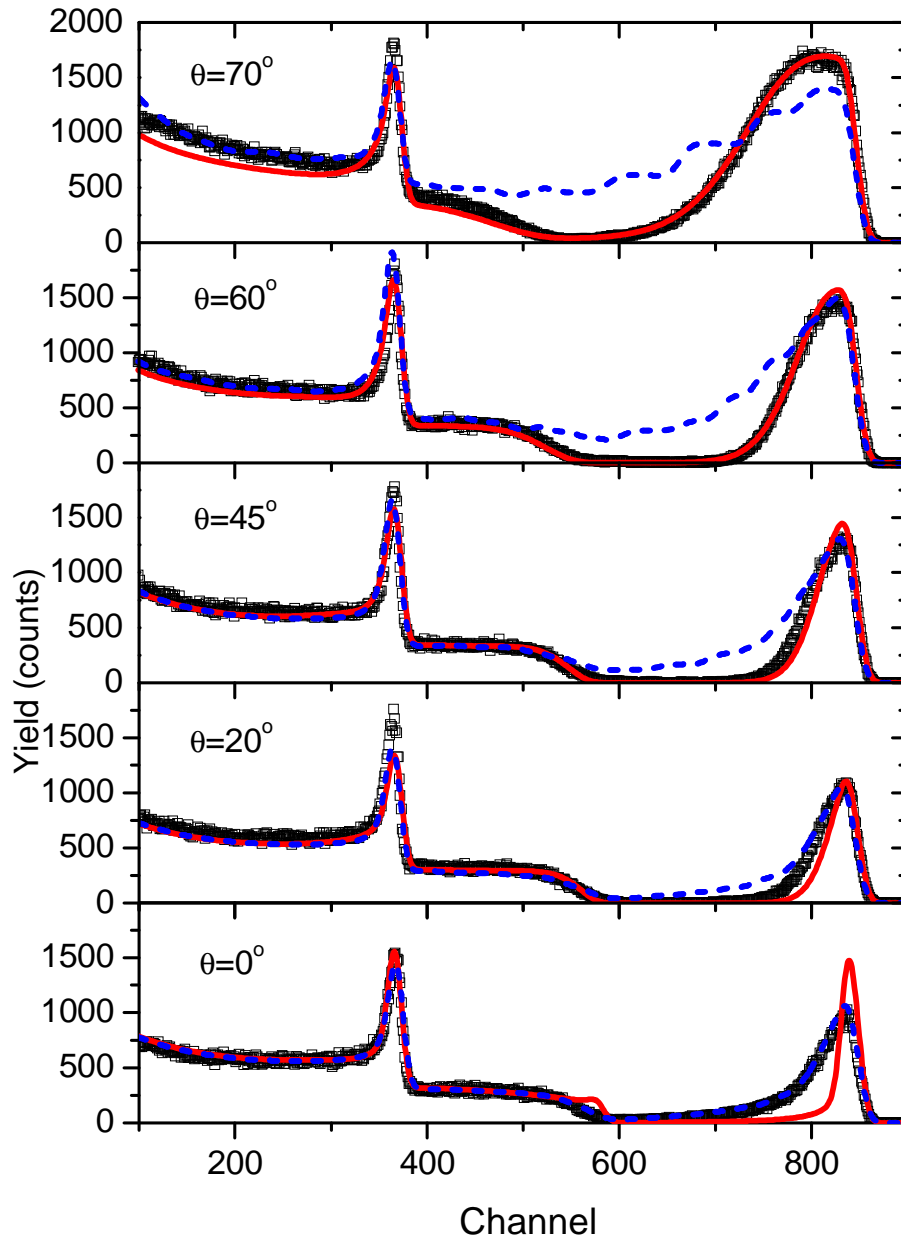


Figure 4. RBS spectra of ZnO nanowire sample B. Solid lines: simulation with nanowire model.

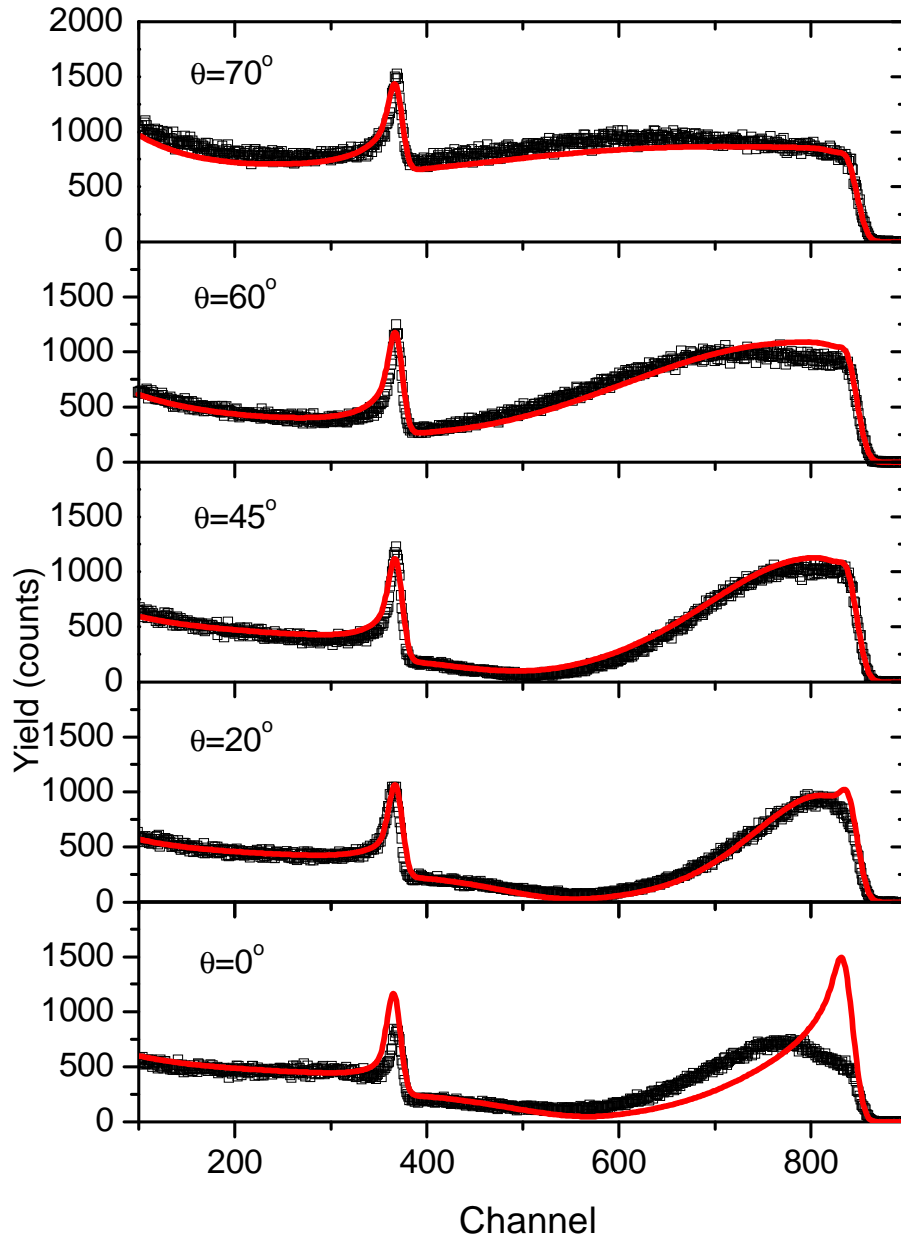


Figure 5. Thickness distribution of an assumed rough ZnO layer that leads to a simulation of the normal incidence RBS spectra of sample A (shown in Figure 3) and sample B (shown in Figure 4).

